A crack closure system for cementitious composite materials using knotted shape memory polymer (k-SMP) fibres

Riccardo Maddalena [a,*], Lorenzo Bonanno [b], Brunella Balzano [a], Cristina Tuinea-Bobe [c], John Sweeney [c], Iulia Mihai [a]

[a] *Cardiff University, School of Engineering, Cardiff, CF24 3AA, UK*
[b] *University of Trento, Department of Civil, Environmental and Mechanical Engineering, Trento, 38123, Italy*
[c] *University of Bradford, Faculty of Engineering and Informatics, Department of Mechanical and Energy Systems Engineering, Bradford, BD7 1DP, UK*

ABSTRACT

Formation of cracks represents one of the major causes of concrete deterioration, which can lead to durability and safety issues. In this work, a novel crack closure system is developed, using polyethylene terephthalate (PET) polymer fibres embedded in a mortar mix. The PET polymer has shape memory properties and shrinks upon thermal activation, if free to do so, or otherwise exerts shrinkage restraint forces. A single knot was manufactured at each end of the PET fibres to provide mechanical anchorage into the mortar matrix. Mortar samples with embedded knotted fibres were pre-cracked and subsequently placed in an oven to thermally activate the polymers and induce the shrinkage mechanism into the fibres. Crack closure was measured in the range 45–100%, depending on the geometry, dimension and distribution of the fibres, and the size of the initial crack.

1. Introduction

Concrete is one of the most used construction materials. Its strength, versatility and its unique combination with steel reinforcement makes it a strong and long-lasting option for the construction industry worldwide [1]. However, the long-term performance of cement bound materials may be compromised, due to their susceptibility to cracking, which is directly linked to their low tensile strength.

Mechanical loading and environmental conditions may lead to the development of tensile stresses in concrete structural elements. When these exceed the tensile strength of the concrete, cracks will develop. The formation of cracks may compromise the overall mechanical performance of a structure, providing easy access for the ingress of water and other agents which may result in the corrosion of reinforcing steel or deterioration of other components [2].

To minimise the negative effect of cracks, the concept of self-healing concrete, i.e. concrete which is able to repair itself without human intervention, has emerged as a possible solution to enhance the durability of concrete structures. Many techniques have been developed over the years, with the aim to provide concrete structures with self-healing capacity [3]. Two strategies for the promotion of self-healing have proven effective. One approach, known as autonomous healing, explores the use of technologies containing self-healing agents (e.g. micro-capsules, super absorbent polymers, bacteria etc.) embedded in the cementitious matrix [4,5], while the other strategy, known as autogenous healing, relies on self-healing compounds intrinsic to the cementitious material [6]. The underlying mechanism in the autogenous healing is characterised by chemical processes that take place when water and/or carbon dioxide infiltrate the cracks; (i) water can react with unhydrated pozzolanic particles and precipitate in additional calcium (aluminum) silicate hydrate, or (ii) the carbon dioxide may react with the existing portlandite and precipitate in calcite [7,8]. Autogenous healing has clear economical advantages over autonomous healing technologies, however its efficiency is restricted to small cracks with openings below a certain limit. Various values have been reported in the literature for the limiting crack width above which autogenous healing no longer takes place, with the majority of studies putting it in the range of 50–150 μm [5,9,10].

The addition of steel or plastic fibres into concrete has been shown to control and reduce cracking [11]. Extensive research has been carried out in the last few decades on the development of fibre reinforced cementitious composites (FRCCs) in order to improve the cracking resistance and the mechanical performance of concrete [12]). The addition of randomly distributed short fibres in a cementitious matrix

---

introduces crack-bridging mechanisms, governed by the debonding and pull-out of the fibres from the cementitious matrix, which in turn result in better crack control, improved post-fracture mechanical behaviour and increased toughness [13,14]. Significantly improved cracking behaviour can be achieved with the use of high-performance fibre reinforced cementitious composites (HPFRCC) which exhibit ductile strain-hardening tensile behaviour and are usually accompanied by extensive multiple micro-cracking up to high levels of strains, before the development of a localised macro-crack [12,15,16]. The formation of multiple cracks with reduced openings and the delay in the development of macro-cracks can lead to reduced ingress of air, water and harmful agents through the network of cracks [17,18], with a positive effect on durability. Smaller crack openings achieved by the use of fibres can also result in substantial autogenous healing due to the ability of cement to further hydrate and precipitate more crystalline phases between the two crack surfaces [19–22]. Recent studies on the self-healing capability of ultra-HPFRCC have shown that, under cryogenic conditions [23], high aspect ratio straight steel fibres contributed to a complete crack closure after water curing [24].

The bond between the fibres and the cementitious matrix is a key factor that influences the crack-bridging action of fibres [13]. Improving this bond by providing hooked ends to the fibres, carefully modifying the fibre-matrix interface properties or adopting an undulating (or crimped) fibre profile was shown to enhance the pull-out resistance of fibres and the overall crack-bridging behaviour [12,25,26].

While initial work focused more on steel fibres, research has also been conducted on the use of other fibre materials, such as plastic, macro-synthetic, rubbers and engineered polymers [21,27–32]. One particular class of engineered polymers are shape memory polymers (SMP), characterised by their ability to respond to external stimuli by altering their physical shape [33,34]. During manufacture, these polymers are deformed (e.g. stretched) and then cooled such that they have a temporary (or fixed) shape [35,36]. The new temporary shape will remain stable unless the polymer is exposed to an external stimulus that triggers the recovery of the original shape [37]. Polyethylene terephthalate (PET) is a thermo-responsive shape memory polymer. During production, the PET is pre-drawn at an elevated temperature, and the previously random long chain molecules are aligned and stretched. The aligned molecular configuration is then fixed by cooling but can be released by reheating above the glass transition temperature. SMP PET filaments bundled into tendons previously employed in crack-closure systems in concrete [38,39]. By applying heat onto the tendons to activate their shape memory response (shrinking), these systems were shown to be effective in closing cracks with openings of 0.3 mm. Whilst the manufacture of this crack closure technology has been combined with secondary pre-stressing elements [40], the system requires an external source of heat to induce the polymers to shrink.

Nevertheless, particular engineering applications do exist [41–43] in which concrete elements can be subjected to temperature variations compatible with the heat requirements for crack closure systems involving heat activation of SMPs.

In oil and gas extraction wells, the downhole temperature can exceed 110 °C [41,44]. Cement is used to protect and seal the borehole wall to prevent any interaction between soil-aquifer systems and the pumped fluid [45]. The isolation of liquid and gases extracted from the well is found to be the main issue in well integrity, and recent studies have reported a rate of failure of up to 10% [46]. Throughout its service life, the oil well structure is subjected to temperature and pressure fluctuations that can lead to crack formation and compromise the oil well integrity. Extensive research has been carried out on improving mechanical performance and durability of oil well cements, using additives, fibres and alternative cementitious materials [47–50], but both durability and effective monitoring remain challenges [51–54]. To control crack widths, SMP filaments could be employed in oil well cementitious structures where the heat produced by the extracted fluid activates the polymers embedded in the matrix.

Other engineering applications where a secondary heat source can be explored as an activation means for SMP-based crack closure systems are within the nuclear industry; concrete and cement composites are used in low- and intermediate-level waste immobilisation and encapsulation and secondary barriers [55]. Such types of waste release heat at temperatures in the range of 180–200 °C for several decades [42].

Concrete is also employed in the fabrication of reinforced concrete pipes for the transportation of high temperature fluids in chemical engineering plants [43]. Thermal gradient between the fluid and the outer surface of the pipe could lead to cracking and through these cracks, fluids and gasses may leak into the surrounding environment [56]. The presence of SMP elements within the matrix could control the crack width and prevent any leak by thermal activation using the heat of the fluids itself.

In this paper, a novel crack closure system is described that employs SMP fibres embedded in lab-scale mortar beams. Fibres are knotted at both ends to create a mechanical anchor and subsequently mixed in with the mortar. When the fibres are thermally activated their end-anchorage enables the development of shrinkage stresses, i.e. tensile stresses that develops in an SMP fibre when it is activated under restrained conditions [38]. If the two knots of a fibre lie either side of a crack, they will apply compression on the crack faces. Therefore, in the proposed system, the crack closure mechanism relies on this shrinkage stress, achieved by providing an effective mechanical anchorage at the fibre ends. This is in contrast to the crack-bridging mechanism in conventional FRCCs, generally governed by fibre pull-out.

In order to study the crack closure potential of knotted SMP fibres, mortar beams with different distributions and orientations of fibres were cast. The beams were notched, pre-cracked under three-point bending and then oven heated to activate the shrinkage mechanism in the PET fibres. The crack width was measured before and after the thermal activation of the fibres. The conceptual model is presented in Fig. 1.

2. Materials and methods

2.1. Materials

2.1.1. Mortar paste

Cement mortar was prepared using ordinary Portland cement CEM II A/L 32.5 R, standard quartz sand used as fine aggregate, and tap water. Cement (c) and sand (s) were mixed at a c/s ratio of 1:3 by mass, and water (w) was added at a w/c ratio of 0.5 by mass. The mix proportions of cement, sand and water were 480.5 kg/m^3, 1441.3 kg/m^3 and 240.2 kg/m^3 respectively. The sand was sieved to isolate the particle fraction <2 mm. Material characteristics are reported in Table 1.

2.1.2. k-SMP fibres

The shape memory polymer (SMP) fibres used in this work were manufactured at the University of Bradford (UK) from commercial grade polyethylene terephthalate (PET), Dow Lighter C93, in granular form. Fibres were obtained by melt extrusion first, followed by die-drawing to achieve molecular orientation in the fibres [39,57,58]. The precise processing conditions have been reported previously [39]. The final diameter of the fibres was 0.95 mm, corresponding to a draw ratio of 4.0, under a draw rate of 1000 mm/min. The measured density of the fibre is 1.31 g/cm^3.

The PET filaments were tested to evaluate their thermomechanical properties. A single PET filament of 200 ± 1 mm was clamped in an Avery Denison tensile machine, and then loaded at a rate of 0.5 mm/s, at room temperature, and subjected to load until failure. The stress-strain curves for three nominal similar filament samples (filament A, filament B and filament C) are shown in Fig. 2. The filaments showed an average stress at failure of approximately 257 MPa (coefficient of variation, CV = 8%) and an average strain at failure of 5%. Those values are in agreement with the results shown in previous studies, where the same PET materials was used [39,58]. The shrinkage potential was measured
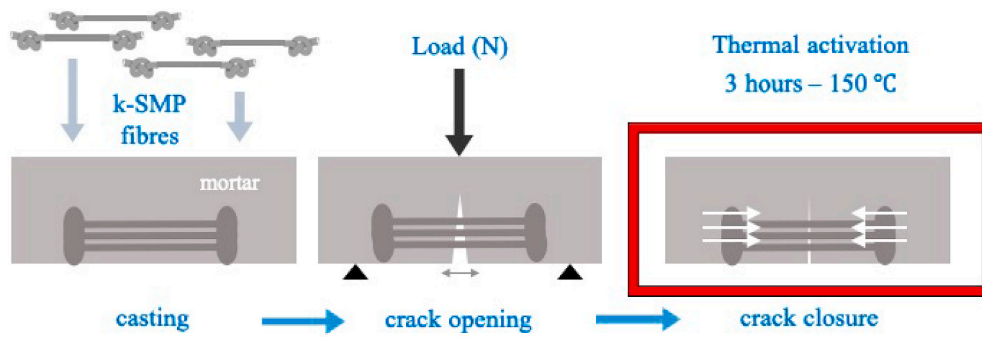
Fig. 1. Conceptual model of the k-SMP fibres technology for crack closure in cementitious systems.

Table 1

Characteristic of mortar components: CEM II A/L (Class 32,5 R), according to the certificate of conformity, test method BS EN 197–1:2011, and sand.

Components	CEM II	Sand (< 2 mm)
	%	%
Clinker	96	–
Gypsum added	4.0	–
Chemical composition		
SiO2	17.06	99.9
Al2O3	3.96	traces
Fe2O3	3.09	traces
CaO	63.91	–
MgO	2.13	–
SO3	3.01	–
Na2O	0.17	–
L.O.I.	6.39	–
Density (kg/m3)	3300	2500

Fig. 3. Development of restrained shrinkage stresses in heated SMP filaments at target temperatures of 90, 100 and 150 C° [Solid lines indicate the shrinkage stress as a function of time; dashed lines indicate the temperature profile as a function of time].
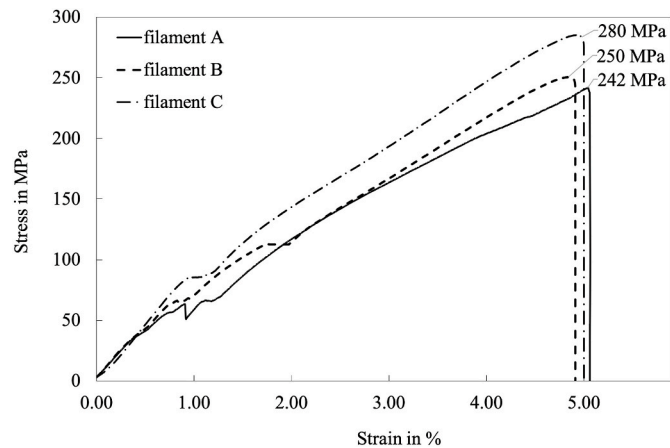

Fig. 2. Tensile behaviour of SMP filaments.

under restrained and free conditions. In the first case, a single filament of 200 ± 1 mm was clamped in a heated cell, and while the temperature was increased to a target value of 90, 100 and 150 °C, the stress developed due to the restrained shrinkage was measured. When the filament was heated to a target temperature of 150 °C, the peak stress measured was 46 MPa, compared to peak stress values of 34 MPa and 36 MPa measured when the specimens were heated to peak temperatures of 100 and 90 °C respectively. Details of the measurements are reported in Fig. 3.

The free shrinkage was measured using filaments of 100 ± 1 mm in effective length ($L_{f.eff}$), placed in a pre-heated oven at 100, 120 and 150 °C for 10, 20 and 30 min respectively. The average shrinkage (in %), as a mean value for three different specimens at each selected time and
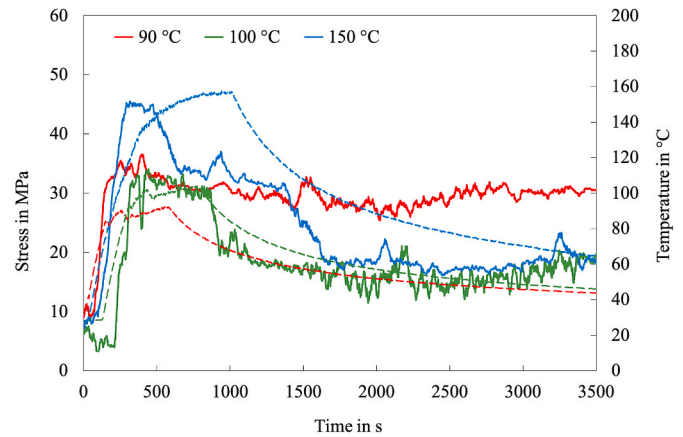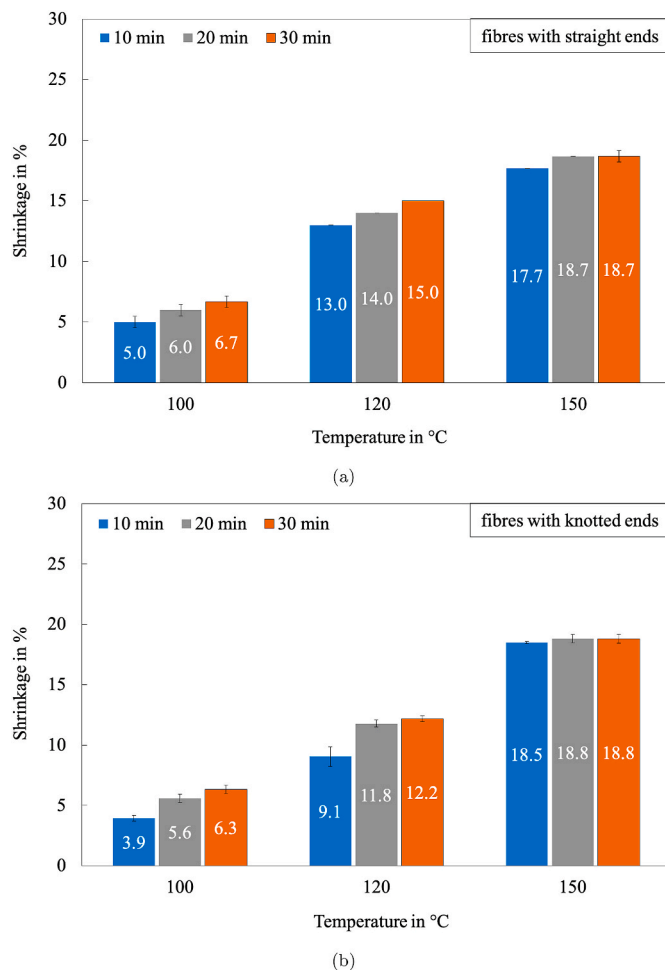
temperature, for fibres with straight and knotted ends is reported in Fig. 4a and Fig. 4b, respectively. The relatively low values of standard deviation ensure a good degree of reproducibility. The highest temperature of 150 °C results in the greatest shrinkage of approximately 18%, and the presence of the knots does not influence the shape memory effect.

The effectiveness of the knots in providing the fibres with a mechanical anchorage into the mortar matrix was assessed by means of a testing procedure similar to a conventional pull-out test. The pull-out response of fibres with knotted ends was compared with that of fibres with straight ends.

Both ends of individual fibres were cast in $25 \times 25 \times 25$ mm mortar cubes, in an arrangement that provided an embedment length of $L_{f.emb} = 20 \pm 1$ mm at each fibre end, as shown in Fig. 5a and Fig. 5b. The cubes encasing the fibre ends were then cured for 7 days at room temperature. The cubes were cased between steel platens, as shown in Fig. 5c. A cork sheet of 2 mm thickness was placed between the mortar cube and the steel platen to reduce local crushing of the fine asperities on the mortar surface. A tensile load was applied under displacement control at a rate of 0.3 mm/s.

The samples with straight ends failed at load levels of 10–30 N (Fig. 6) by complete pull-out. Their load values are much lower than those of steel fibres [59], but comparable to those of polypropylene (PP) fibres and PET fibres studied by Di Maida et al. [60], and Khalid et al. [61] respectively. The knotted fibres were able to withstand much higher levels of load, in the range of 230–290 N, as shown in Fig. 6. All samples failed by fibre rupture in the midspan, rather than pull-out, with elongations up to 10–12 mm. Whilst these load values are similar to the pull-out load of steel fibres [24,62], the failure mechanism is different.

(a)

(b)

Fig. 4. Free shrinkage potential of (a) fibres with straight ends and (b) fibres with knotted ends at different target temperatures (100, 120 and 150 °C) and different heating time (10, 20 and 30 min). The error bars represent the standard deviation.

The mechanical anchorage provided by the knots enabled the fibres to withstand these tensile force levels without pulling out from the matrix.

2.2. Specimen preparation and test methodology

The mortar paste was produced using a standard bowl mixer and procedures according to BS EN 196–1:2016. A summary of the k-SMP fibre-mortar specimens is given in Table 2. Mortar beams were cast into two different moulds, a small one ($160 \times 40 \times 40$ mm) and a large one ($250 \times 75 \times 75$ mm) respectively. Two different specimen designs were employed: small beams with aligned fibres (AD), as shown in Fig. 8a, and large beams with a random distribution and orientation of fibres (RD), as reported in Fig. 8b. The fibre content and orientation in the two different types of specimens are described by the volume fraction (V_f) and the fibres orientation factor (α) respectively, as detailed in sections 2.2.1 and 2.2.2. The PET fibres were manually cut and a single knot was tied at both ends of each fibre. Two different fibre lengths were employed; fibres with an effective length of $L_{f,eff} = 55 \pm 1$ mm were used in the RD specimens and fibres with an effective length of $L_{f,eff} = 100 \pm 1$ mm were employed in the AD specimens, noting that $L_{f,eff}$ represents the length of the fibre in between the two end-knots, as detailed in Fig. 7. Six AD specimens and five RD specimens were cast. In both series (AD and RD), the fibres were oiled using moulding oil prior to incorporating them in the mortar matrix, in order to prevent a chemical bond forming. It must be noted that during casting no bleeding was observed.

2.2.1. Specimens with aligned fibre distribution (AD)

k-SMP fibres with an effective length $L_{f,eff} = 100$ mm were used to produce six AD specimens. The fibres for the AD series were manufactured by cutting 160 mm long segments of PET filament and tying a single knot at each end. A total of 30 fibres were placed only in the bottom half of each AD beam as follows: one layer of mortar (5 mm in thickness) was poured in the mould followed by one layer of 10 k-SMP fibres, placed along the length of the mould and equally spaced across its breadth. This procedure was repeated three times, with the fibres being placed in three layers below the neutral axis of the mortar beam, as shown in Fig. 8a. A local volume fraction is defined for the AD specimens as the volume fraction in the bottom half of the beam V_B, where the fibres are placed. In this work, the effective length of the fibres is employed in the evaluation of the fibre content and thus, the volume fraction for the AD specimens is $V_{f,AD} = 1.66\%$. Furthermore, a fibre orientation factor, α, defined as the average ratio of the projected fibre length in the tensile stress direction to the fibre length itself [63,64] is employed to describe the orientation of fibres. For the AD specimens, the fibre orientation factor is $\alpha = 1.0$.

2.2.2. Specimens with randomly distributed and oriented fibres (RD)

A total of five specimens ($255 \times 75 \times 75$ mm) containing fibres with a random distribution were cast; fibres with $L_{f,eff} = 55$ mm ($L_{f,tot} = 100$ mm), were added to the mortar paste in the mixer bowl, and mixed together to achieve a homogeneous distribution. The fibre-mortar mix was then poured into steel moulds in three layers, as shown in Fig. 8b. A total of 300 k-SMP fibres were used in each beam leading to a volume fraction $V_{f,RD} = 0.82\%$, based on the effective length of the fibres $L_{f,eff}$.

A fibre orientation factor for the RD specimens of $\alpha = 0.722$ was theoretically evaluated by employing the model proposed by Dupont and Vandewalle [64], which takes into account the significant effect of the boundaries on the fibre orientation but also assumes that the fibres are straight and rigid. Alberti et al. [65] showed that the use of a reduction factor based on the projected chord of a bent fibre is more suitable for synthetic flexible fibres that may fold. Employing the projected folded fibre of $L_{fr} = 0.856\, L_{f,eff}$ of [65] in the model of Dupont and Vandewalle [64], results in a slightly reduced value for the orientation factor, respectively $\alpha = 0.681$.

2.2.3. Crack opening measurements

After 28 days of curing, all specimens were oven-dried at 50 °C for 24 h to remove excess of water that might affect strength measurements [30,66]. A 3 mm wide notch was cut at mid-span into the lower face of AD specimens and a 5 mm wide notch was cut at mid-span into the RD beams. The indentation was cut using an electric saw, with an incision depth of 2 mm and 3 mm respectively in the AD and RD specimens. Knife-edged metal plates were glued to the bottom of the beams either side of the notch to allow the crack mouth opening displacement (CMOD) to be measured using a clip gauge (Fig. 9a). The crack width was measured at 4 different stages, as summarised in Table 3.

All beams were subjected to three-point bending under CMOD control at a displacement rate of 0.01 mm/min (Fig. 9b). Loading was stopped when the macro-crack reached a target CMOD of 0.3 mm and the beams were subsequently unloaded (Fig. 10, stage A in Table 3). The target CMOD of 0.3 mm was chosen in accordance with code requirements [67]. The CMOD values measured by the clip gauge when the beams were fully unloaded were between 0.08 mm and 0.15 mm (stage B). A control specimens of plain mortar (small beam) was also subjected to three-point bending test, however the sample broke apart after reaching the maximum level of load (1.9 kN). After 24 h, the crack width was measured using an optical microscope and a micrometer glass slide (stage C). Values of maximum strength, and strength and crack width values at unloading stage are reported in Table A1 in the Appendix.
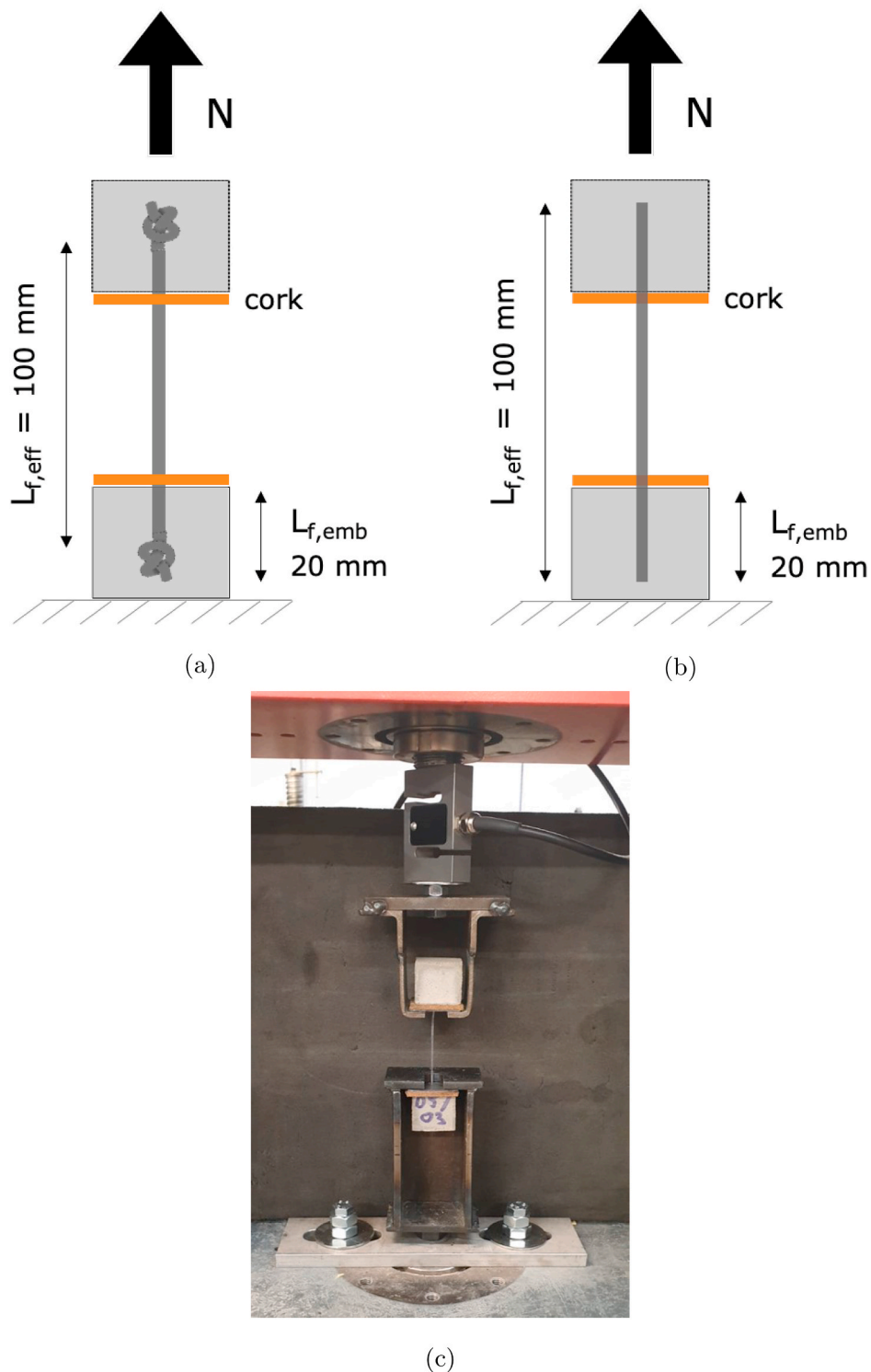
Fig. 5. Test set-up for the resistance of the mechanical anchorage. (a) Fibre with knotted ends. (b) Fibre with straight ends. (c) Sample placed in the test machine.

2.2.4. Microscopy measurements and k-SMP activation

After unloading, the samples were placed horizontally for 24 h before thermal activation. An optical microscope coupled with a 10x Moticam camera was used to measure the crack width before (stage C) and after the thermal activation (stage D). To perform scaled measurements, a calibration glass slide (1 DIV = 0.01 mm) was placed over the crack and used as a reference. It was noticed that the crack width values recorded with the CMOD clip gauge after unloading were consistently larger than the readings of the microscope 24 h after the unloading, for

reasons discussed below.

This observed elastic closure effect is due to the presence of the PET fibres, which continues to contract elastically for some time after the specimens are unloaded and further reduces the crack width. 24 h after unloading, the samples were placed in a pre-heated oven at 150 °C for 3 h in order to activate the shape memory effect in the fibres and cause them to shrink. This was followed by 12 h of air-cooling at room temperature. The crack-widths were measured on both sides of each beam (front-side denoted by *X* and back-side denoted by *Y*) at two different
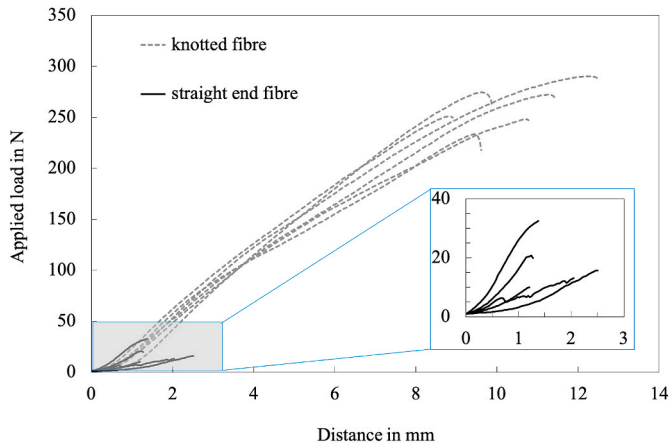
Fig. 6. Anchorage resistance curves for straight-end and knotted fibres.

Table 2
Sample ID for specimens in aligned (AD) and random distribution (RD) design, sample dimensions (height H, width W and length L, in mm), effective fibre length ($L_{f,eff}$) in mm, number of specimens produced, fibre content as volume fraction for AD design ($V_{f,AD}$) and RD design ($V_{f,RD}$), and theoretical orientation factor α.

	H x W x L [mm x mm x mm]	$L_{f,eff}$ [mm]	number of specimens	Fibres content	Theoretical orientation factor
Aligned Distribution				$V_{f,AD}$	α
AD1, AD2, …, AD6	40 × 40 x 160	100	6	1.66%	1.0
Random Distribution				$V_{f,RD}$	α
RD1, RD2, …, RD5	75 × 75 x 255	55	5	0.82%	0.681
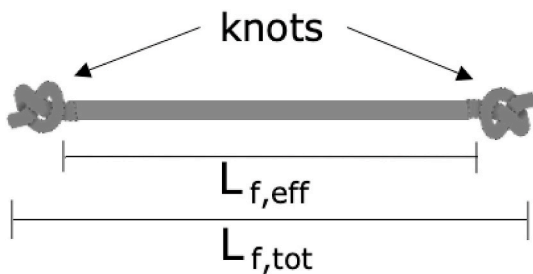
Fig. 7. Detail of k-SMP fibre with knotted ends and effective length, from knot-to-knot.

points as indicated in Fig. 11; measurement #1 at approximately 5 mm above the notched area and measurement #2 in close proximity of it respectively. Measurements were carried out 24 h after unloading, before and after thermal activation, using the same location on the mortar surface. Images of the crack aperture were collected and imported into AutoCAD, then processed to perform scaled measurements, with an accuracy of 0.001 mm.

3. Results and discussion

Crack width measurements obtained before and after thermal activation of the k-SMP fibres, following the procedure described in 2.2.4 are presented and discussed in this section.

After thermal activation, a reduction in crack widths was observed at each sample measurement point, for all AD and RD specimens. At each measurement location the crack closure level was determined as the ratio between the crack width reduction and the original opening, before activation.

Crack width measurements for AD series (6 specimens) carried out before and after thermal activation (stage C and D in Table 3), in both locations (#1 and #2), are reported in Fig. 12a for side *X* and for side *Y*, respectively. Crack width measurements on both sides of the beams at both locations before thermal activation were generally consistent and were found to be in the range of 0.024–0.077 mm (mean = 0.045 mm, Std. Dev. = 0.014 mm). After thermal activation, reduced crack width measurements, in the range of 0–0.025 mm (mean = 0.010 mm, Std. Dev. = 0.007 mm) were obtained (Fig. 12a). Average crack closure levels of 77% (Std. Dev. = 16%) were determined, as shown in Fig. 13a, with some cases of full closure (e.g. sample AD2, AD3 and AD5, Table A2 and Fig. A1a in the Appendix). Example microscopy images of crack aperture for sample AD3 before and after thermal activation are given in Fig. 14a and Fig. 14b respectively.

The larger specimens with random fibres (RD series, 5 specimens) showed a consistent crack opening before thermal activation on both *X*–side and *Y*–side of the beams, as shown in Fig. 12b. The initial crack aperture was measured in the range of 0.068–0.114 mm (mean = 0.092 mm, Std. Dev. = 0.013 mm). After thermal activation, crack widths were recorded in the range of 0.025–0.075 mm (mean = 0.051 mm, Std. Dev. = 0.015 mm), with an average crack closure of approximately 45% (Std. Dev. = 13%), as shown in Fig. 13b and Fig. A2b in the Appendix. Example microscopy images of a crack in RD beams before and after thermal activation are shown in Fig. 14c and Fig. 14d respectively for sample RD5, *Y*–side.

Crack width measurements after activation together with pull-out and restrained shrinkage test results indicate that the presence of the knots embedded in the mortar matrix provide an effective anchorage system which allows significant levels of shrinkage stresses to develop in the fibres resulting in substantial crack closure.

As previously reported in Fig. 3, the peak tensile stress value developed at 150 °C was 45 MPa (equivalent to a peak tensile force of approximately 32 N) and Figs. 2 and 6 suggest that the knotted fibres can withstand these stress levels without breaking or pulling out.

The results presented show that k-SMP filaments are able to reduce crack widths by 77% on average in AD specimens, with some achieving
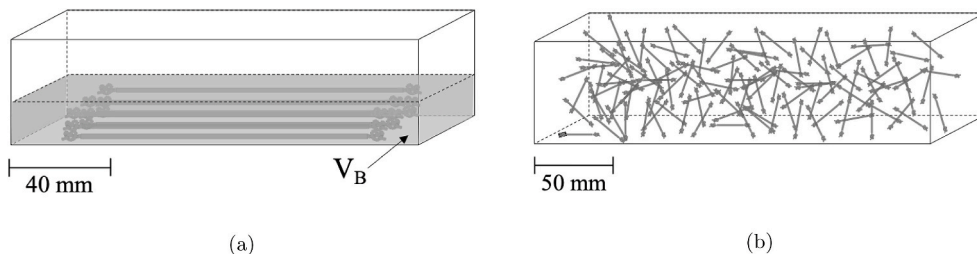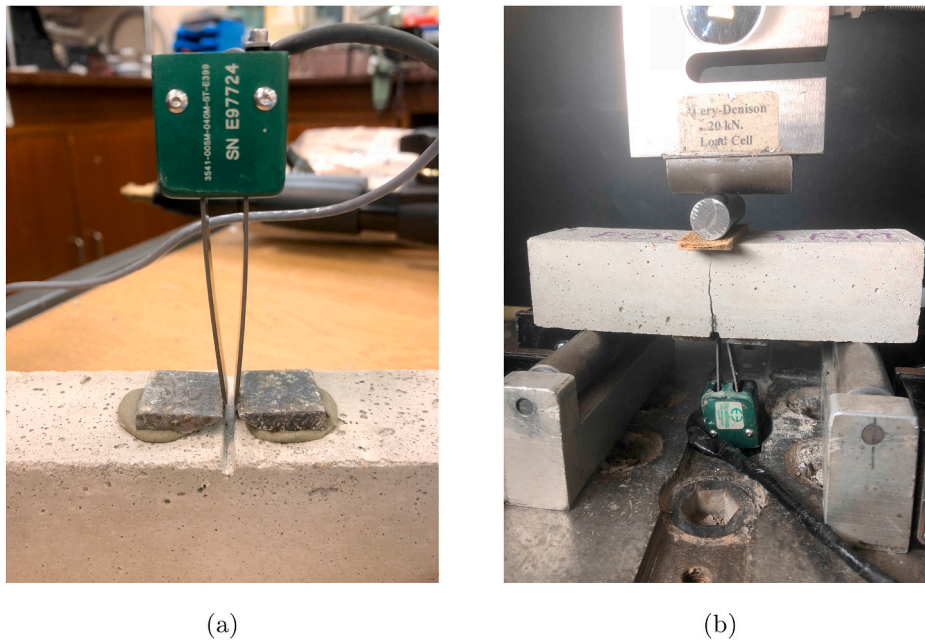

(a)

(b)

Fig. 8. Schematic representation of specimens. (a) beams with aligned distribution of fibres (AD). (b) beams with a random distribution of fibres (RD) [not to scale].

(a)

(b)

Fig. 9. (a) Detail of knife-edge metal bars glued to the beam. (b) three-point bending test setup with CMOD clip gauge in place.

Table 3
Crack-opening measurement stages.

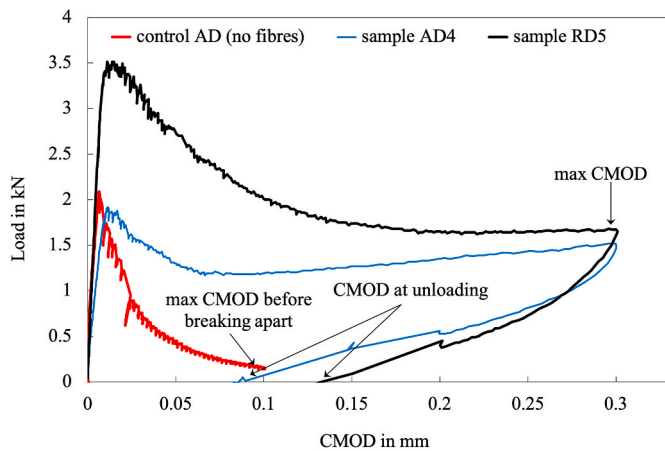|	Stage	Measurement device
A	target CMOD (0.3 mm)	clip gauge
B	at complete unloading	clip gauge
C	unloading, after 24 h rest	microscope
D	12 h after thermal activation	microscope

Fig. 10. Loading curves for samples AD4, RD5 and control AD specimen (plain mortar, beam size 160 × 40 × 40 mm), with CMOD values at max opening and unloading (in stage A and B of Table 3).

similar trend is indicated by the results presented here with respect to crack closure when using k-SMP fibres. All measured residual crack widths after activation (as shown in Fig. 15), for both AD and RD series, are smaller than 150 μm, a level below which the potential for autogenous healing increases greatly [71,72]. This suggests that k-SPM fibres could be used in combination with other stimulated autogenous healing systems to achieve a complete crack healing [3,5].

The complete set of crack widths measurements as well as the crack closure values are provided in the Appendix in Table A2 and Table A3 for AD and RD samples respectively.

The k-SMP fibres also have a significant crack-bridging action, primarily due to the mechanical anchors provided by the knots and by the high tensile strength of fibres. The effect of the k-SMP fibres before thermal activation can be noted in Fig. 10 in which a significant increase in the flexural toughness of k-SMP AD sample relative to that of the control beam (plain mortar) of the same size is observed. Moreover, the k-SMP AD beam exhibits a hardening behaviour after an initial drop in flexural capacity.

The results of the study presented here clearly show the potential of k-SMP fibres in providing an effective crack closure system for cementitious materials. The limited scale of the study was mainly due to the rather time intensive process of knotting the individual fibres manually. The authors acknowledge that a more comprehensive study will be required to fully explore the capabilities of the proposed system and to determine the optimum parameters (e.g. fibre content, fibre geometry, end anchorage etc.) for best performance. To this end, the automated manufacturing of knotted SMP fibres, or indeed SMP fibres with alternative end anchorages, would be extremely beneficial. Knots can be created automatically by a number of methods. The most sophisticated use robotics, such as in surgical applications for suturing [73]. However, much faster and cheaper methods are available commercially, such as in the packaging industry, for which knotting machines are available, such as the automatic high speed hang tag threader machine LM-LY3, manufactured and assembled by Ruian Universal Machinery Co. Ltd., Guangdong, China [74]. Similar technology could be applied to PET fibres, with necessary adaptations to allow for the particular mechanical properties of the oriented polymer. Tags could also be created by methods other than knotting, such as by ultrasonic welding of extra larger sections parts onto the fibre ends. Alternatively, to increase the mechanical anchorage with the matrix, fibres can be deformed by
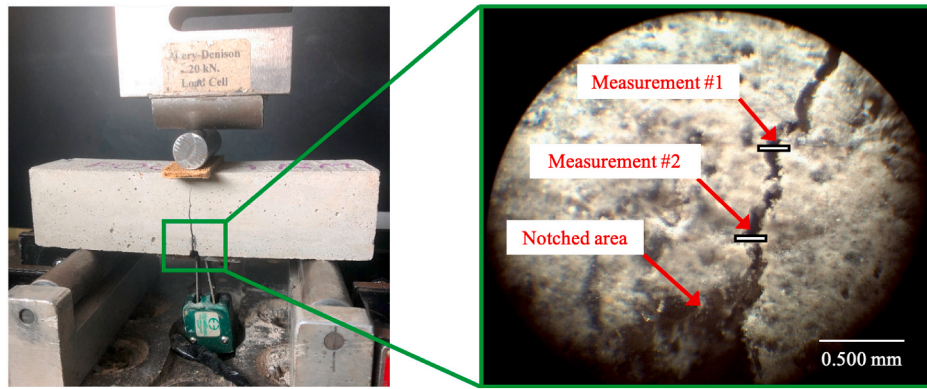
100% closure (as shown in Fig. 12a and Fig. A1a in the Appendix), and by 45% on average in RD specimens (Fig. 13 and Fig. A1a in the Appendix). The better performance observed in the AD specimens is due to a higher local fibre content as well as a more favourable fibre orientation, i.e. perpendicular to the crack surface. The orientation and distribution of fibres was shown to have a strong influence on the mechanical properties and performance of standard fibre reinforced concrete [68–70], with a superior crack resistance and post-cracking strength observed for fibre orientations near perpendicular to cracks [68,69]. A

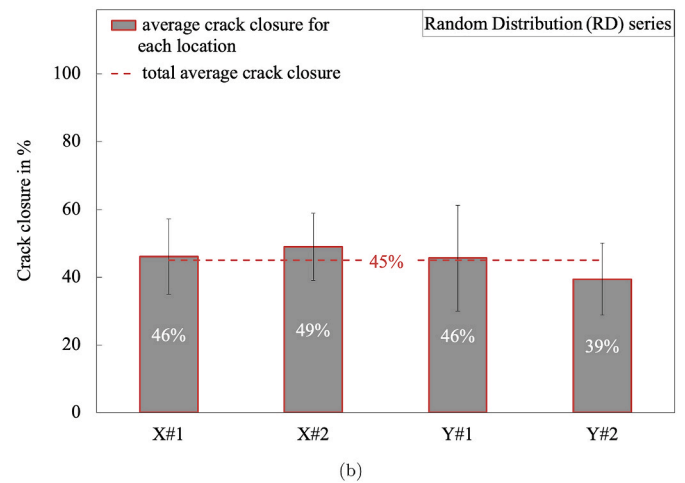**Fig. 11.** Details of the microscope measurements of the crack width (stage C and D in Table 3).
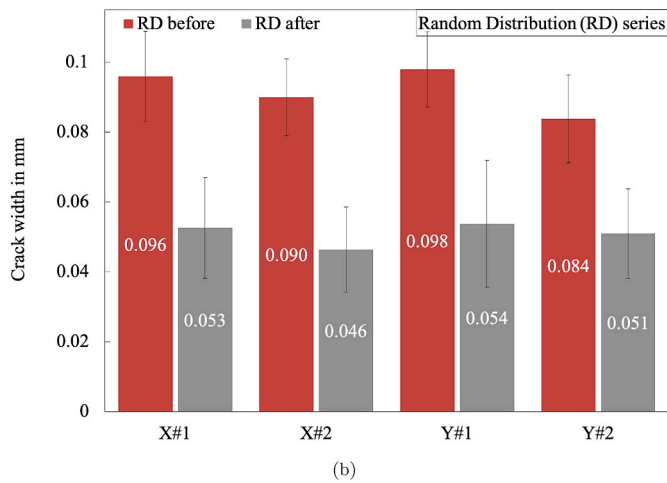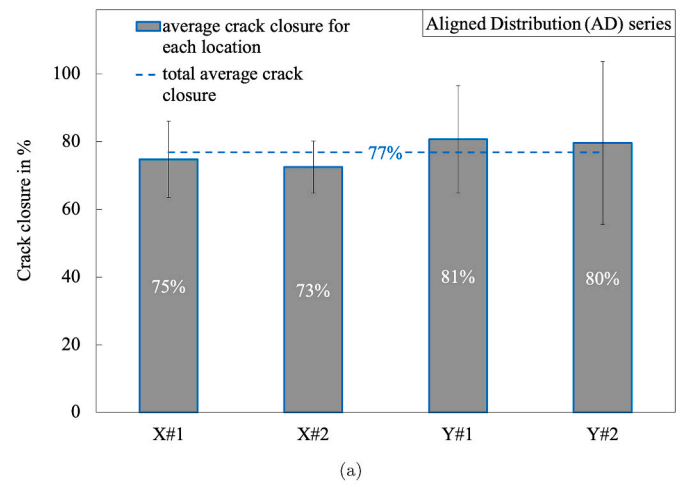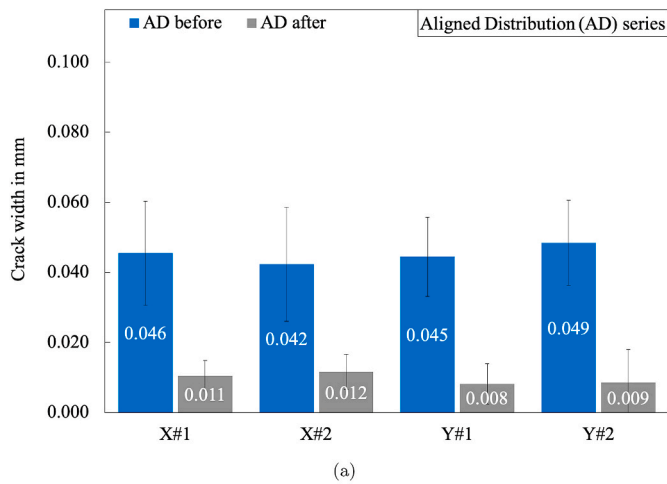

Fig. 12. Average crack widths of samples in (a) aligned distribution samples (AD series) and (b) random distribution (RD series), before and after thermal activation, measured in location #1 and #2 of *X*– and *Y*–side of the beam. The error bars represent the standard deviation.

Fig. 13. Average crack closure values at both sides of the notched area (*X* and *Y*) and both location (i.e. #1 and #2) of (a) samples in aligned distribution (AD series) and (b) samples in random distribution (RD series). The error bars represent the standard deviation.

adding buttons at the end of the fibres [27,75].

In this study, X-CT images were also collected to make qualitative observations of the fibres within the volume surrounding the crack (notched area). X-Ray computer tomography (X-CT) characterisation is a non-destructive technique used to investigate the material internal structure without damaging the original specimen [76]. A μCT Bruker SkyScan was used on a core (75 × 20 × 20 mm) cut from central part of sample RD4 after its thermal activation. X-Ray images were taken with a pixel size resolution of 9 μm, an accelerating voltage of 100 kV and 2736 ms exposure. The 3D reconstruction is shown in Fig. 16 for illustrative purposes. A transversal image (Fig. 16, *green plane*, and Fig. 17a) with respect to the *y*-axis shows the k-SMP fibre embedded in the mortar. A magnified portion of 30 × 30 mm reported in Fig. 17b) shows a k-SMP filament bridging a macro-crack after its thermal activation. The image features the orientation effect of the fibre (with respect to the *y*– and *z*–dimensions), and the folding effect, as discussed in section 2.2.2.
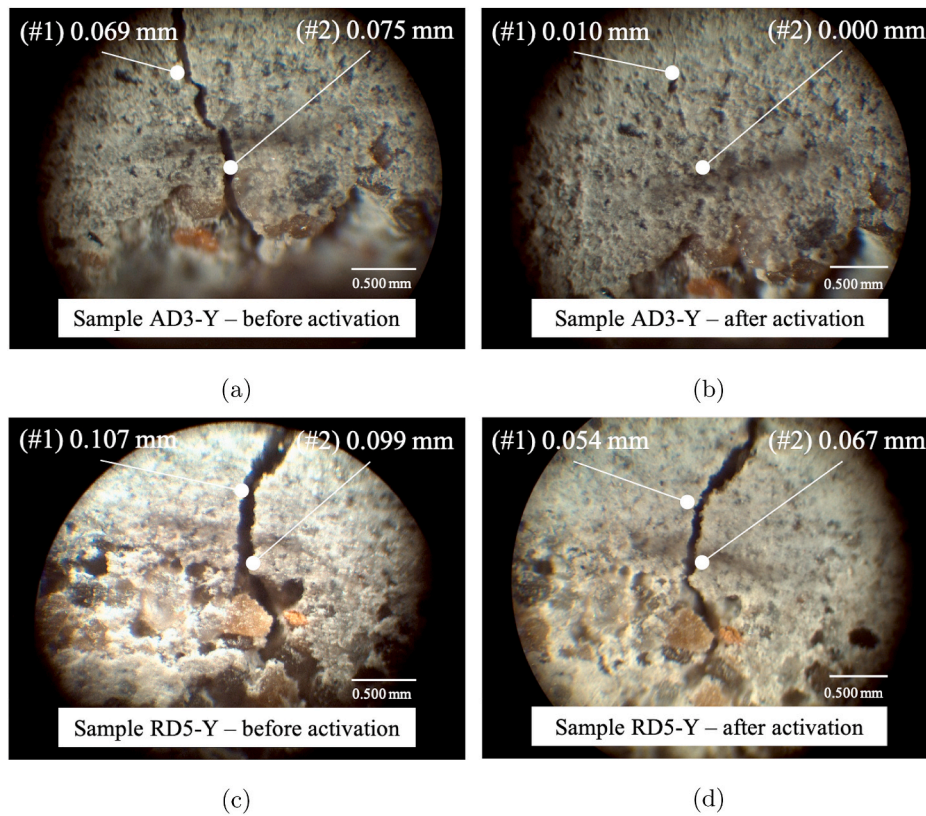
(a)

(b)

(c)

(d)

Fig. 14. Microscope images of crack width measurements of sample AD3, *Y*–side, (a) before thermal activation and (b) after thermal activation, and ample RD5, *Y*–side, (c) before thermal activation and (d) after thermal activation.
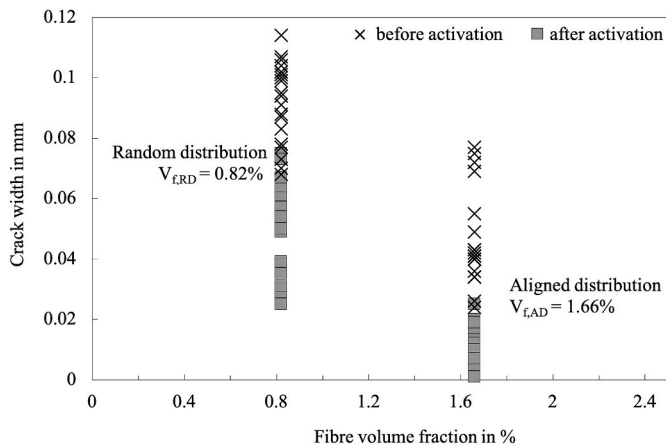

Fig. 15. Crack widths before and after thermal activation for RD and AD series respectively, as a function of the fibre volume fraction.

Fig. 16. 3D reconstruction of a section (75 × 20 × 20 mm) of sample RD4.

X-CT imaging analysis could be employed to provide valuable information regarding the orientation and distribution of fibres [77,78], detection of internal cracks, the build up of self-healing products inside the cracks. etc. [79,80]. Such a comprehensive analysis is outside the scope of this study however, it could play an important role in the further development of the crack closure system presented here.

The proposed novel crack closure system employing k-SMP fibres was shown to be effective in reducing openings of previously formed cracks and it is envisaged that it could be exploited as a solution in improving durability. The k-SMP fibres could provide a self-healing mechanism reducing crack widths, therefore protect the concrete steel reinforcement from air and water entrainment and subsequent
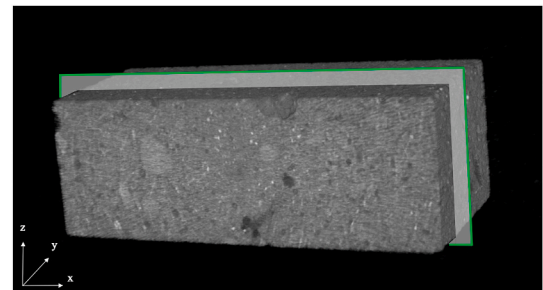
corrosion. While other SMP-concrete composite technologies may require an external heat source to activate the shape memory effect [33, 36,38,39,58], the k-SMP fibres could be used in engineering applications, with intrinsic heat emission; e.g. oil-well cements, where the heat within the pumped fluid could be used for thermal activation [81,82]. Other such applications are within the nuclear waste storage sector, where low and intermediate-level waste are encapsulated in concrete shells and nuclear by-products release heat at temperature in the range of 180–200 °C for several decades [42].

4. Conclusions

In this work a novel crack closure system for cementitious materials was presented. Shape memory PET fibres were embedded in a mortar paste. Fibres were manufactured with a single knot (k-SMP) at both ends, to enhance bonding with the cement paste. Samples were cast with either aligned (AD) or randomly distributed (RD) fibres, cured for 28 days and pre-cracked at mid-span. The initial target crack width value of
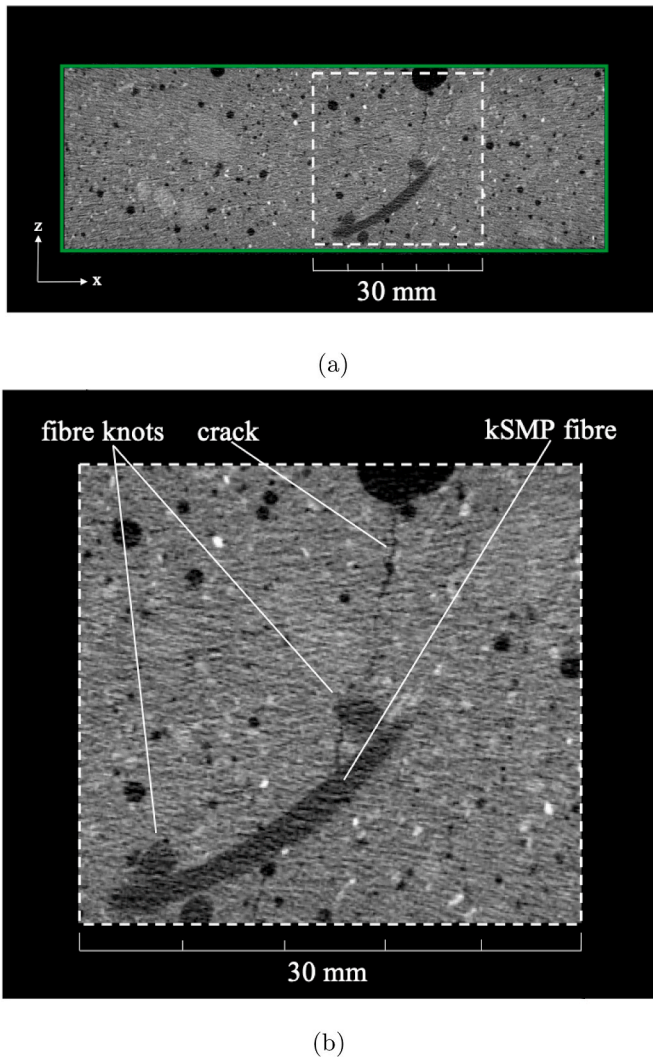
Fig. 17. X-CT image of (a) section of the sample RD4 after thermal activation and (b) magnification with detail of k-SMP fibre and crack.

0.3 mm was controlled using a crack mouth opening displacement (CMOD) clip gauge placed in the notched area. Crack widths were measured before and after thermal activation using an optical microscope and the crack closure levels were calculated.

The following conclusions can be drawn:

- Samples with aligned fibres (AD), and fibre content of 1.66%, showed successful average crack closure levels of 77%, with some samples exhibiting full crack closure (100%).
- Samples with random distribution (RD) and fibre content of 0.56%, showed average crack closure levels of 45%, up to a maximum of 69%.
- The knots provided effective mechanical end-anchorage for the fibres, allowing restrained shrinkage induces tensile stresses to develop upon thermal activation.
- k-SMP fibres also provide significant crack-bridging action.

This novel crack closure system is shown to be promising and it could be combined with other self-healing technologies (i.e. micro-capsules, crystalline admixtures, SAPs [83–85]) to achieve full crack-healing and stiffness recovery.

Further work will focus on the optimisation of fibre geometry, content and end anchorage as well as an automated manufacturing process for large scale production of the fibres. Knots on PET filaments can be created automatically by using robotics or knotting machine [73,74]. The mechanical anchorage given by the knot could be provided by creating tags or adding buttons at the end of the fibres [27,75]. An automated manufacturing process is essential in investigating the performance of k-SMP fibres on larger scale specimens as well as the fresh state properties (i.e. workability, bleeding, distribution and orientation of fibres, etc.).

Declaration of competing interest

The authors declare that they have no known competing financial interests or personal relationships that could have appeared to influence the work reported in this paper.

Appendix. Supplementary data

Supplementary data (Appendix) to this article can be found online at https://doi.org/10.1016/j.cemconcomp.2020.103757.

References

[1] L. Basheer, J. Kropp, D.J. Cleland, Assessment of the durability of concrete from its permeation properties: a review, Construct. Build. Mater. 15 (2) (2001) 93–103, https://doi.org/10.1016/S0950-0618(00)00058-1.

[2] A.R. Suleiman, M.L. Nehdi, Effect of environmental exposure on autogenous self-healing of cracked cement-based materials, Cement Concr. Res. 111 (2018) 197–208, https://doi.org/10.1016/j.cemconres.2018.05.009.

[3] L. Ferrara, T.V. Mullem, M. Cruz, P. Antonaci, R. Paul, E. Cuenca, A. Jefferson, P.-l. Ng, A. Peled, M. Roig-flores, M. Sanchez, C. Schroefl, P. Serna, D. Snoeck, J. Marc, N.D. Belie, Experimental characterization of the self-healing capacity of cement based materials and its effects on the material performance: a state of the art report by COST Action SARCOS WG2, Construct. Build. Mater. 167 (2018) 115–142, https://doi.org/10.1016/j.conbuildmat.2018.01.143.

[4] A. Al-tabbaa, B. Lark, K. Paine, T. Jefferson, C. Litina, D. Gardner, T. Embley, Biomimetic Cementitious Construction Materials for Next-Generation Infrastructure, Proceeding of the Institution of Civil Engineers - Smart Infrastructure and Construction, 2018, p. 1, https://doi.org/10.1680/jsmic.18.00005.

[5] N. De Belie, E. Gruyaert, A. Al-Tabbaa, P. Antonaci, C. Baera, D. Bajare, A. Darquennes, R. Davies, L. Ferrara, T. Jefferson, C. Litina, B. Miljevic, A. Otlewska, J. Ranogajec, M. Roig-Flores, K. Paine, P. Lukowski, P. Serna, J.-M. Tulliani, S. Vucetic, J. Wang, H.M. Jonkers, A review of self-healing concrete for damage management of structures, Advanced Materials Interfaces 5 (17) (2018), 1800074, https://doi.org/10.1002/admi.201800074.

[6] Y. Yang, E.-H. Yang, V.C. Li, Autogenous healing of engineered cementitious composites at early age, Cement Concr. Res. 41 (2) (2011) 176–183, https://doi.org/10.1016/J.CEMCONRES.2010.11.002. https://www.sciencedirect.com/science/article/pii/S0008884610002346.

[7] K. Van Tittelboom, E. Gruyaert, H. Rahier, N. De Belie, Influence of mix composition on the extent of autogenous crack healing by continued hydration or calcium carbonate formation, Construct. Build. Mater. 37 (2012) 349–359, https://doi.org/10.1016/j.conbuildmat.2012.07.026.

[8] E. Gruyaert, K. Van Tittelboom, H. Rahier, N. De Belie, Activation of pozzolanic and latent-hydraulic reactions by alkalis in order to repair concrete cracks, J. Mater. Civ. Eng. 27 (7) (2015) 1–12, https://doi.org/10.1061/(ASCE)MT.1943-5533.0001162.

[9] M. Sahmaran, G. Yildirim, T.K. Erdem, Self-healing capability of cementitious composites incorporating different supplementary cementitious materials, Cement Concr. Compos. 35 (1) (2013) 89–101, https://doi.org/10.1016/j.cemconcomp.2012.08.013.

[10] X. Wang, C. Fang, D. Li, N. Han, F. Xing, A self-healing cementitious composite with mineral admixtures and built-in carbonate, Cement Concr. Compos. 92 (2018) 216–229, https://doi.org/10.1016/j.cemconcomp.2018.05.013.

[11] A. Brandt, Fibre reinforced cement-based (FRC) composites after over 40 years of development in building and civil engineering, Compos. Struct. 86 (1–3) (2008) 3–9, https://doi.org/10.1016/j.compstruct.2008.03.006.

[12] A.E. Naaman, Half a century of progress leading to ultra-high performance fiber reinforced concrete: part 1-overall review, in: 2nd Int. RILEM Conference on Strain

Hardening Cementitious Composites, RILEM, Rio de Janeiro, 2011, pp. 12–14. http://demo.webdefy.com/rilem-new/wp-content/uploads/2016/10/9a5f35e31c44c6654fea693290c512e8.pdf.

[13] A. Bentur, S. Mindess, Fibre Reinforced Cementitious Composites, Taylor & Francis, 2007. https://www.crcpress.com/Fibre-Reinforced-Cementitious-Composites/Bentur-Mindess-outledge/p/book/9780415250481.

[14] E. Cuenca, L. Ferrara, Self-healing capacity of fiber reinforced cementitious composites. State of the art and perspectives, KSCE Journal of Civil Engineering 21 (7) (2017) 2777–2789, https://doi.org/10.1007/s12205-017-0939-5. http://link.springer.com/10.1007/s12205-017-0939-5.

[15] V.C. Li, On engineered cementitious composites (ECC), J. Adv. Concr. Technol. 1 (3) (2003) 215–230, https://doi.org/10.3151/jact.1.215. http://joi.jlc.jst.go.jp/JST.JSTAGE/jact/1.215?from=CrossRef.

[16] S. Paul, S. Pirskawetz, G. van Zijl, W. Schmidt, Acoustic emission for characterising the crack propagation in strain-hardening cement-based composites (SHCC), Cement Concr. Res. 69 (2015) 19–24, https://doi.org/10.1016/J.CEMCONRES.2014.12.003. https://www.sciencedirect.com/science/article/pii/S0008884614002452.

[17] V. Marcos-Meson, A. Michel, A. Solgaard, G. Fischer, C. Edvardsen, T.L. Skovhus, Corrosion resistance of steel fibre reinforced concrete - a literature review, Cement Concr. Res. 103 (2018) 1–20, https://doi.org/10.1016/J.CEMCONRES.2017.05.016.

[18] V. Marcos-Meson, G. Fischer, C. Edvardsen, T. Skovhus, A. Michel, Durability of Steel Fibre Reinforced Concrete (SFRC) exposed to acid attack – a literature review, Construct. Build. Mater. 200 (2019) 490–501, https://doi.org/10.1016/J.CONBUILDMAT.2018.12.051.

[19] D. Homma, H. Mihashi, T. Nishiwaki, Self-healing capability of fibre reinforced cementitious composites, J. Adv. Concr. Technol. 7 (2) (2009) 217–228.

[20] V.C. Li, E. Herbert, Robust self-healing concrete for sustainable infrastructure, J. Adv. Concr. Technol. 10 (6) (2012) 207–218, https://doi.org/10.3151/jact.10.207.

[21] T. Nishiwaki, S. Kwon, D. Homma, M. Yamada, H. Mihashi, Self-healing capability of fiber-reinforced cementitious composites for recovery of watertightness and mechanical properties, Materials 7 (2014) 2141–2154, https://doi.org/10.3390/ma7032141.

[22] H. Liu, Q. Zhang, C. Gu, H. Su, V. Li, Influence of microcrack self-healing behavior on the permeability of engineered cementitious composites, Cement Concr. Compos. 82 (2017) 14–22, https://doi.org/10.1016/J.CEMCONCOMP.2017.04.004.

[23] J.J. Kim, D.Y. Yoo, Effects of fiber shape and distance on the pullout behavior of steel fibers embedded in ultra-high-performance concrete, Cement Concr. Compos. 103 (2019) 213–223, https://doi.org/10.1016/j.cemconcomp.2019.05.006.

[24] M.J. Kim, D.Y. Yoo, Cryogenic pullout behavior of steel fibers from ultra-high-performance concrete under impact loading, Construct. Build. Mater. 239 (2020), 117852, https://doi.org/10.1016/j.conbuildmat.2019.117852.

[25] Z. Lin, V.C. Li, Crack bridging in fiber reinforced cementitious composites with slip-hardening interfaces, J. Mech. Phys. Solid. 45 (5) (1997) 763–787, https://doi.org/10.1016/S0022-5096(96)00095-6. https://www.sciencedirect.com/science/article/pii/S0022509696000956.

[26] L. Soufeiani, S.N. Raman, M.Z.B. Jumaat, U.J. Alengaram, G. Ghadyani, P. Mendis, Influences of the volume fraction and shape of steel fibers on fiber-reinforced concrete subjected to dynamic loading – a review, Eng. Struct. 124 (2016) 405–417, https://doi.org/10.1016/J.ENGSTRUCT.2016.06.029.

[27] S. Singh, A. Shukla, R. Brown, Pullout behavior of polypropylene fibers from cementitious matrix, Cement Concr. Res. 34 (10) (2004) 1919–1925, https://doi.org/10.1016/j.cemconres.2004.02.014.

[28] D. Snoeck, K. Van Tittelboom, S. Steuperaert, P. Dubruel, N. De Belie, Self-healing cementitious materials by the combination of microfibres and superabsorbent polymers, J. Intell. Mater. Syst. Struct. 25 (1) (2014) 13–24, https://doi.org/10.1177/1045389X12438623. http://journals.sagepub.com/doi/10.1177/1045389X12438623.

[29] A.J. Babafemi, W.P. Boshoff, Tensile creep of macro-synthetic fibre reinforced concrete (MSFRC) under uni-axial tensile loading, Cement Concr. Compos. 55 (2015) 62–69, https://doi.org/10.1016/j.cemconcomp.2014.08.002.

[30] S.Z. Qian, J. Zhou, E. Schlangen, Influence of curing condition and precracking time on the self-healing behavior of engineered cementitious composites, Cement Concr. Compos. 32 (9) (2010) 686–693, https://doi.org/10.1016/j.cemconcomp.2010.07.015.

[31] D. Snoeck, N. De Belie, From straw in bricks to modern use of microfibers in cementitious composites for improved autogenous healing - a review, Construct. Build. Mater. 95 (2015), https://doi.org/10.1016/j.conbuildmat.2015.07.018.

[32] D. Wang, Y. Ju, H. Shen, L. Xu, Mechanical properties of high performance concrete reinforced with basalt fiber and polypropylene fiber, Construct. Build. Mater. 197 (2019) 464–473, https://doi.org/10.1016/J.CONBUILDMAT.2018.11.181.

[33] W. Huang, Z. Ding, C. Wang, J. Wei, Y. Zhao, H. Purnawali, Shape memory materials, Mater. Today 13 (7–8) (2010) 54–61, https://doi.org/10.1016/S1369-7021(10)70128-0.

[34] M.D. Hager, S. Bode, C. Weber, U.S. Schubert, Shape memory polymers: past, present and future developments, Prog. Polym. Sci. 49–50 (2015) 3–33, https://doi.org/10.1016/J.PROGPOLYMSCI.2015.04.002.

[35] Y. Zhou, W.M. Huang, Shape memory effect in polymeric materials: mechanisms and optimization, Procedia IUTAM 12 (2015) 83–92, https://doi.org/10.1016/J.PIUTAM.2014.12.010.

[36] F. Pilate, A. Toncheva, P. Dubois, J.-M. Raquez, Shape-memory polymers for multiple applications in the materials world, Eur. Polym. J. 80 (2016) 268–294, https://doi.org/10.1016/J.EURPOLYMJ.2016.05.004.

[37] T. Xie, Recent advances in polymer shape memory, Polymer 52 (22) (2011) 4985–5000, https://doi.org/10.1016/J.POLYMER.2011.08.003.

[38] A. Jefferson, C. Joseph, R. Lark, B. Isaacs, S. Dunn, B. Weager, A new system for crack closure of cementitious materials using shrinkable polymers, Cement Concr. Res. 40 (5) (2010) 795–801, https://doi.org/10.1016/J.CEMCONRES.2010.01.004.

[39] O. Teall, M. Pilegis, J. Sweeney, T. Gough, G. Thompson, A. Jefferson, R. Lark, D. Gardner, Development of high shrinkage polyethylene terephthalate (PET) shape memory polymer tendons for concrete crack closure, Smart Mater. Struct. 26 (4) (2017), 045006, https://doi.org/10.1088/1361-665X/aa5d66.

[40] B. Balzano, Enhanced concrete crack closure with hydrid shape memory polymer tendons, in: G. Pijaudier-Cabot, P. Grassl, C. La Borderie (Eds.), 10th International Conference on Fracture Mechanics of Concrete and Concrete Structures FraMCoS-X, 2019, pp. 1–5, https://doi.org/10.21012/fc10.235142.

[41] W. Renpu, Production casing and cementing, in: Advanced Well Completion Engineering, third ed., Elsevier, 2011, pp. 221–294, https://doi.org/10.1016/B978-0-12-385868-9.00009-9. Ch. 5.

[42] C. Ferry, C. Poinssot, C. Cappelaere, L. Desgranges, C. Jegou, F. Miserque, J. P. Piron, D. Roudil, J.M. Gras, Specific outcomes of the research on the spent fuel long-term evolution in interim dry storage and deep geological disposal, J. Nucl. Mater. 352 (1–3) (2006) 246–253, https://doi.org/10.1016/j.jnucmat.2006.02.061.

[43] Z. Zhang, H. Wang, Alkali-activated cements for protective coating of OPC concrete, in: Handbook of Alkali-Activated Cements, Mortars and Concretes, Elsevier, 2015, pp. 605–626, https://doi.org/10.1533/9781782422884.4.605. Ch. 22.

[44] M.A. Grant, P.F. Bixley, Production testing, in: Geothermal Researvoir Engineering, second ed., Elsevier, 2011, pp. 131–168, https://doi.org/10.1016/B978-0-12-383880-3.10008-3. Ch. 8.

[45] T. Bennett, Well Cement Integrity and Cementing Practices, Tech. Rep, The University of Adelaide, Adelailde AUS, 2016.

[46] R.B. Jackson, The integrity of oil and gas wells, Proc. Natl. Acad. Sci. Unit. States Am. 111 (30) (2014) 10902–10903, https://doi.org/10.1073/pnas.1410786111.

[47] M. Choolaei, A. Morad, M. Ardjmand, A. Yadegari, H. Soltanian, The effect of nanosilica on the physical properties of oil well cement, Mater. Sci. Eng., A 538 (2012) 288–294, https://doi.org/10.1016/j.msea.2012.01.045.

[48] J.D. Mangadlao, P. Cao, R.C. Advincula, Smart cements and cement additives for oil and gas operations, J. Petrol. Sci. Eng. 129 (2015) 63–76, https://doi.org/10.1016/j.petrol.2015.02.009.

[49] C. Wang, X. Chen, X. Wei, R. Wang, Can nanosilica sol prevent oil well cement from strength retrogression under high temperature? Construct. Build. Mater. 144 (2017) 574–585, https://doi.org/10.1016/j.conbuildmat.2017.03.221.

[50] N. Jafariesfad, M. Khalifeh, P. Skalle, M. Rica, Nanorubber-modified cement system for oil and gas well cementing application, J. Nat. Gas Sci. Eng. 47 (2017) 91–100, https://doi.org/10.1016/j.jngse.2017.10.002.

[51] S. Ridha, S. Irawan, B. Ariwahjoedi, Strength prediction of Class G oilwell cement during early ages by electrical conductivity, Journal of Petroleum Exploration and Production Technology 3 (4) (2013) 303–311, https://doi.org/10.1007/s13202-013-0075-9.

[52] C. Vipulanadna, A. Mohammed, Nanoparticle modified smart oil well cement for monitoring cementing applications, in: American Association of Drilling Engineering, 2015, pp. 1–16. No. June 2016.

[53] Q. Wu, M. Dininger, S. Nair, E. van Oort, A. Guzik, K. Kishida, Real time cement displacement tracking using distributed fiber optic sensors, in: SPE Annual Technical Conference and Exhibition, Society of Petroleum Engineers, 2017, pp. 1–12, https://doi.org/10.2118/187409-MS.

[54] C. Vipulanandan, A. Mohammed, Smart Cement Modified with Laponite for Real Time Monitoring of Oil Well Cementing Applications, in: 2017 AADE National Technical Conference and Exhibition, American Association of Drilling Engineers, Houston, 2017, pp. 1–11. AADE-17-NTCE-126 Smart.

[55] J. Kotatkova, J. Zatloukal, P. Reiterman, K. Kol, Concrete and cement composites used for radioactive waste deposition, J. Environ. Radioact. 179 (2017) 147–155, https://doi.org/10.1016/j.jenvrad.2017.08.012.

[56] S. Lee, Y. Park, A. Abolmaali, Investigation of flexural toughness for steel-and-synthetic-fiber-reinforced concrete pipes, Structure 19 (2019) 203–211, https://doi.org/10.1016/j.istruc.2018.12.010. January.

[57] P.D. Coates, I.M. Ward, Die drawing: solid phase drawing of polymers through a converging die, Polym. Eng. Sci. 21 (10) (1981) 612–618, https://doi.org/10.1002/pen.760211007.

[58] O. Teall, M. Pilegis, R. Davies, J. Sweeney, T. Jefferson, R. Lark, D. Gardner, A shape memory polymer concrete crack closure system activated by electrical current, Smart Mater. Struct. 27 (7) (2018), 075016, https://doi.org/10.1088/1361-665X/aac28a.

[59] D.Y. Yoo, H.J. Choi, S. Kim, Bond-slip response of novel half-hooked steel fibers in ultra-high-performance concrete, Construct. Build. Mater. 224 (2019) 743–761, https://doi.org/10.1016/j.conbuildmat.2019.07.099.

[60] P. Di Maida, E. Radi, C. Sciancalepore, F. Bondioli, Pullout behavior of polypropylene macro-synthetic fibers treated with nano-silica, Construct. Build. Mater. 82 (2015) 39–44, https://doi.org/10.1016/j.conbuildmat.2015.02.047.

[61] F.S. Khalid, J.M. Irwan, M.H. Wan Ibrahim, N. Othman, S. Shahidan, Splitting tensile and pullout behavior of synthetic wastes as fiber-reinforced concrete, Construct. Build. Mater. 171 (2018) 54–64, https://doi.org/10.1016/j.conbuildmat.2018.03.122.

[62] H. Zhang, T. Ji, X. Lin, Pullout behavior of steel fibers with different shapes from ultra-high performance concrete (UHPC) prepared with granite powder under different curing conditions, Construct. Build. Mater. 211 (2019) 688–702, https://doi.org/10.1016/j.conbuildmat.2019.03.274.

[63] P. Soroushian, C.-D. Lee, Distribution and orientation of fibers in steel fiber reinforced concrete, ACI Mater. J. 87 (5) (1990) 433–439.

[64] D. Dupont, L. Vandewalle, Distribution of steel fibres in rectangular sections, Cement Concr. Compos. 27 (3) (2005) 391–398, https://doi.org/10.1016/j.cemconcomp.2004.03.005.

[65] M.G. Alberti, A. Enfedaque, J.C. Gálvez, How to predict the orientation factor of non-rigid macro-synthetic fibre reinforced concrete, IOP Conf. Ser. Mater. Sci. Eng. 246 (1) (2017), https://doi.org/10.1088/1757-899X/246/1/012030.

[66] X. Chen, W. Huang, J. Zhou, Effect of moisture content on compressive and split tensile strength of concrete, Indian J. Eng. Mater. Sci. 19 (2012) 427–435.

[67] EN 1992-1-1: Eurocode 2: Design of Concrete Structures - Part 1-1: General Rules and Rules for Buildings, Tech. rep (2004).

[68] L. Vandewalle, G. Heirman, F. Van Rickstal, Fibre orientation in self-compacting fibre reinforced concrete, in: 7th International RILEM Symposium on Fibre Reinforced Concrete, RILEM, Chennai, 2008, pp. 719–728.

[69] O. Švec, G. Žirgulis, J.E. Bolander, H. Stang, Influence of formwork surface on the orientation of steel fibres within self-compacting concrete and on the mechanical properties of cast structural elements, Cement Concr. Compos. 50 (2014) 60–72, https://doi.org/10.1016/j.cemconcomp.2013.12.002.

[70] H. Li, R. Mu, L. Qing, H. Chen, Y. Ma, The influence of fiber orientation on bleeding of steel fi ber reinforced cementitious composites, Cement Concr. Compos. 92 (2018) 125–134, https://doi.org/10.1016/j.cemconcomp.2018.05.018.

[71] H.-w. Reinhardt, M. Jooss, Permeability and self-healing of cracked concrete as a function of temperature and crack width, Cement Concr. Res. 33 (2003) 981–985, https://doi.org/10.1016/S0008-8846(02)01099-2.

[72] B. Isaacs, R. Lark, T. Jefferson, R. Davies, S. Dunn, Crack healing of cementitious materials using shrinkable polymer tendons, Struct. Concr. 14 (2) (2013) 138–147, https://doi.org/10.1002/suco.201200013.

[73] D.L. Chow, R.C. Jackson, C.M. Cavusotlu, W. Newman, A novel vision guided knot-tying method for autonomous robotic surgery, IEEE International Conference on Automation Science and Engineering (2014) 504–508, https://doi.org/10.1109/CoASE.2014.6899373.

[74] High speed hang tag threader machine LM-LY3. http://www.universalmachinery.com.cn/products/high-speed-hang-tag-threader-machine-lm-ly3-ID190.html.

[75] A.E. Naaman, S.P. Shah, J.L. Throne, Some Developments in Polypropylene Fibers for Concrete, Publication SP - American Concrete Institute, 1984, pp. 375–396.

[76] E.N. Landis, D.T. Keane, X-ray microtomography, Mater. Char. 61 (12) (2010) 1305–1316, https://doi.org/10.1016/j.matchar.2010.09.012.

[77] K.J. Trainor, B.W. Foust, E.N. Landis, Measurement of energy dissipation mechanisms in fracture of fiber-reinforced ultrahigh-strength cement-based composites, J. Eng. Mech. 139 (7) (2013) 771–779, https://doi.org/10.1061/(ASCE)EM.1943-7889.0000545.

[78] E. Landis, G. Gangsa, L. Flanders, Nanoscratch simulation on a copper thin film using a novel multiscale model, Journal of nanomechanics and micromechanics 6 (4) (2016), 04016007–4016011–04016007–8. doi:10.1061/(ASCE)NM.

[79] E.N. Landis, E.N. Nagy, D.T. Keane, Microstructure and fracture in three dimensions, Eng. Fract. Mech. 70 (7–8) (2003) 911–925, https://doi.org/10.1016/S0013-7944(02)00157-1.

[80] X.F. Wang, Z.H. Yang, C. Fang, N.X. Han, G.M. Zhu, J.N. Tang, F. Xing, Evaluation of the mechanical performance recovery of self-healing cementitious materials – its methods and future development: a review, Construct. Build. Mater. 212 (2019) 400–421, https://doi.org/10.1016/j.conbuildmat.2019.03.117.

[81] K.J. Krakowiak, J.J. Thomas, S. Musso, S. James, A.-t. Akono, F.-j. Ulm, Nano-chemo-mechanical signature of conventional oil-well cement systems: effects of elevated temperature and curing time, Cement Concr. Res. 67 (2015) 103–121, https://doi.org/10.1016/j.cemconres.2014.08.008.

[82] M.I. Childers, M.-t. Nguyen, K.A. Rod, P.K. Koech, W. Um, J. Chun, V.-a. Glezakou, D. Linn, T.J. Roosendaal, T.W. Wietsma, N.J. Huerta, B.G. Kutchko, C. A. Fernandez, Polymer-cement composites with self-healing ability for geothermal and fossil energy applications, Chem. Mater. (2017), https://doi.org/10.1021/acs.chemmater.7b00344.

[83] C.D. Nardi, A. Cecchi, L. Ferrara, A. Benedetti, D. Cristofori, Effect of age and level of damage on the autogenous healing of lime mortars, Composites Part B 124 (2017) 144–157, https://doi.org/10.1016/j.compositesb.2017.05.041.

[84] P. Giannaros, A. Kanellopoulos, A. Al-Tabbaa, Sealing of cracks in cement using microencapsulated sodium silicate, Smart Mater. Struct. 25 (8) (2016), https://doi.org/10.1088/0964-1726/25/8/084005.

[85] D. Snoeck, N. De Belie, Repeated autogenous healing in strain-hardening cementitious composites by using superabsorbent polymers, J. Mater. Civ. Eng. 28 (1) (2016), 04015086, https://doi.org/10.1061/(ASCE)MT.1943-5533.0001360.